Progress In Electromagnetics Research C, Vol. 44, 145–159, 2013

RESEARCH ON VESSEL AND CHAFF ECHO CHARACTERISTICS FOR WIDEBAND COHERENT RADAR

Bo Liu* **and Wenge Chang**

College of Electronic Science and Engineering, National University of Defense Technology, Changsha, Hunan 41007, P. R. China

Abstract—To study effective anti-chaff jamming methods, this paper investigates the echo characteristics of the vessel and the chaff for missile-borne wideband coherent radars. Firstly, the echo model of the missile-borne wideband coherent LFM pulses radar is built, and the range-Doppler image of the echoes is derived. Based on the measured data, the differences of the echoes between the vessel and the chaff are analyzed. Then in terms of the spread feature and energy evenness of the range-Doppler image, two features of the radar echoes are proposed to distinguish the vessel and chaff. Finally, statistical distributions of the two features are investigated, and we find that the proposed features can be used for chaff jamming identification and suppression.

1. INTRODUCTION

Among the defensive measures against anti-ship missiles, chaff is probably the oldest, but still an effective measure [1]. Besides, compared to other countermeasures, chaff is inexpensive and easy to implement. Consequently, it is widely used by Naval Force all the same. Anti-chaff jamming technology has gained much attention among radar engineers in the past decades. Due to the working environment, however, anti-chaff jamming performance of the missile-borne terminal guidance radar is still imperfect [2]. Some investigations have been proposed to distinguish the target and chaff echoes [3–6]. Generally speaking, the existing anti-chaff jamming methods include the polarization method, time domain correlation method, Doppler spectra method, and time-frequency analysis method. Nevertheless, the polarization method is only at the theoretical analysis stage, and a complex full-polarization terminal guidance radar system is

Received 5 August 2013, Accepted 22 September 2013, Scheduled 30 September 2013
* Corresponding author: Bo Liu (liubo19830120@163.com).

impractical. The performances of the time domain correlation method and Doppler spectra method are both unstable. Time-frequency analysis method seems to have excellent performance, but it usually consumes too much computation, which makes it not suitable for missile-borne radar signal processing. Wideband radar has the ability of high range resolution, which provides us a new technological approach for anti-chaff jamming. In addition, the coherent radar is usually used to restrict clutter and jamming echoes by Doppler analysis. Wideband coherent LFM pulses radar has combination advantages of wideband radar and coherent radar. Furthermore, it has a long coverage and low peak power, which produce a low probability of intercept and strong anti-interference performance [7]. As a result, wideband coherent LFM pulses radar has been widely used in terminal guidance. To study effective anti-chaff jamming methods, the paper investigates the echo characteristics of the vessel and chaff for wideband coherent radars with the background of anti-ship terminal guidance.

There are three main modes of use for chaff at sea [8]. The first mode is known as distraction decoy dispensed by rockets and shells at ranges up to 2 km from the vessel, and a pattern of several rockets fired in different directions to provide alternative targets to missiles. The second is the dump mode which is used closer to the vessel (less than 1 km away), and the chaff fired as a false target to the attacking missile. The third one is the centroid mode, used very close to the ship where the chaff cloud is dispensed at a range of 100–400 m. A large echoing area must be formed in a few seconds and the chaff cloud appears initially near the ship. After the ship moves and is away from the tracking beam of the guidance radar, the chaff cloud puzzles the missile. In the distraction decoy and dump mode, the echoes of the chaff and vessel are in different beams, or in different range cells of the same beam of the missile-borne radar. In the centroid mode, nevertheless, the echoes of the chaff and vessel are in the same range cells of the same beam. In this paper, we focus on the echo characteristics of the chaff in the distraction decoy and (or) the dump mode for wideband LFM coherent pulses radars. Firstly, we build the echo model of the missile-borne wideband coherent radars, and the range-Doppler image of the echoes is derived. For wideband coherent radars, the vessel and the chaff are both range-spread targets. Moreover, due to different velocities of the scatterers, the echo is spread in Doppler as well. Hence for wideband coherent radar, the target is named as a range-Doppler spread target in this work. With the measured data, we analyze the differences of the echoes between the vessel and the chaff. Furthermore, we propose two features of the range-Doppler image to distinguish the vessel and the chaff. And finally, we investigate the

statistical distributions of the two features, and some available results are obtained.

The paper is organized as follows. In Section 2, the echo model of the missile-borne wideband coherent radar is built. In Section 3, based on the range-Doppler image we propose two features to discriminate the vessel and the chaff. The statistical distributions of the proposed features are investigated in Section 4. At last, in Section 5, some conclusions are given.

2. RADAR ECHO MODEL

The transmitted signal of wideband LFM coherent pulses radar is [9]:

$$s\left(\hat{t}, t_s\right) = rect\left(\frac{\hat{t}}{T_p}\right) \cdot \exp(j\pi\mu\hat{t}^2) \cdot \exp(j2\pi f_c t) \tag{1}$$

where

$\hat{t}$: fast time;
M: number of chirp pulses in the train;
T_r: pulse repetition interval (PRI);
t_s: slow time, $t_s = mT_r$, $m = 0, 1, \ldots, M-1$;
t: absolute time, $t = \hat{t} + t_s$;
B: bandwidth of the chirp pulse;
T_p: pulse width;
μ: frequency slope, $\mu = B/T_p$;
f_c: carrier frequency.

According to the multiple main scatterers theory [10], the range-scattering function of a static range-spread target can be expressed as:

$$CF(t) = \sum_{k=1}^{k=K} a_k \cdot \exp\left(j2\pi\varphi_k\right) \cdot \delta(t - \tau_k) \tag{2}$$

where K is the number of scattering centers of the range-spread target. a_k, ϕ_k and τ_k are the amplitude, initial phase and delay of the k-th physical scatterer of the range-spread target in range cells, respectively.

Assuming that the radar is working on the tracking condition and moving towards the target, the radial velocity between the radar and the target remains constant during a coherent processing interval (CPI). Accordingly, the instantaneous range between the radar and the target is:

$$R_k(t_s) = R_{k0} - v_k \cdot t_s, \quad k = 1, 2, \ldots, K. \tag{3}$$

where $R_k(\cdot)$ represents the instantaneous range of the k-th scatterer of the range-spread target, and R_{k0} and v_k are the initial range and

the radial velocity of the k-th scatterer, respectively. Substituting (3) into (2), the instantaneous range-scattering function of a range-spread target is obtained:

$$CF(t,t_s) == \sum_{k=1}^{k=K} a_k \cdot \exp\left(j2\pi\varphi_k\right) \cdot \delta\left[t - \frac{2(R_{k0} - v_k \cdot t_s)}{c}\right] \tag{4}$$

where c is the speed of light.

According to the wideband radar theory [11], the target echo is the convolution of the transmitted signal with the range-scattering function of the target. Therefore, the target echo of the missile-borne wideband radar is expressed as:

$$\begin{aligned} r(\hat{t},t_s) \;=\; & s(\hat{t},t_s) * CF(t,t_s) = \sum_{k=1}^{k=K} a_k \\ & \cdot \exp\left(j2\pi\varphi_k\right) \cdot rect\left[\frac{\hat{t} - 2(R_{k0} - v_k \cdot t_s)/c}{T_p}\right] \\ & \cdot \exp\left\{j\pi\mu\left[\hat{t} - 2(R_{k0} - v_k \cdot t_s)/c\right]^2\right\} \\ & \cdot \exp\left\{j2\pi(f_c + f_{kd})\left[t - (R_{k0} - v_k \cdot t_s)/c\right]\right\} \end{aligned} \tag{5}$$

where $f_{kd} = 2v_k f_c/c$ is the Doppler frequency of the k-th scatterer, $*$ represents the convolution. After mixing and low-pass filtering, the baseband signal is written as:

$$\begin{aligned} r_{baseband}(\hat{t},t_s) = & \sum_{k=1}^{k=K} a_k \cdot \exp\left(j2\pi\varphi_k\right) \cdot rect\left[\frac{\hat{t} - 2(R_{k0} - v_k \cdot t_s)/c}{T_p}\right] \\ & \cdot \exp\left\{j\pi\mu\left[\hat{t} - 2(R_{k0} - v_k \cdot t_s)/c\right]^2 + \underbrace{j2\pi f_{kd} \cdot t}_{\text{time-frequency coupling}}\right\} \\ & \cdot \exp\left[-j4\pi f_c(R_{k0} - v_k \cdot t_s)/c\right] \end{aligned} \tag{6}$$

From (6), it can be seen that the relative radial velocity between the radar and the target produces time-frequency coupling term to the chirp signal [12], which results in mismatching between the target echo and the matched filter. Additionally, the radial velocity between the missile-borne radar platform and the target results in range migration between the echo pulses during a CPI, which may produce detrimental effect on the coherent integration. In practical application, the effect from the time-frequency coupling and the range migration could be restricted at utmost by radar parameters design, or it could be solved by motion compensation method [13]. Here we assume that the effect

on the target echoes resulted from the high speed motion of the radar platform has been properly removed. After matched filtering to the baseband echoes, high range resolution profiles (HRRP) of the target can be obtained:

$$\begin{aligned} y(n,m) &= \sum_{k=1}^{k=K} a_k \sqrt{\mu T_p^2} \cdot rect\left[\frac{nT_s - 2(R_{k0} - v_k \cdot mT_r)/c}{T_p}\right] \\ &\quad \cdot \mathrm{Sinc}\left\{\pi B_c \left[nT_s - \frac{2(R_{k0} - v_k \cdot mT_r)}{c}\right]\right\} \\ &\quad \cdot \exp\left[j2\pi\left(\varphi_k + \frac{1}{8}\right)\right] \cdot \exp\left(-j4\pi f_c \cdot \frac{R_{k0} - v_k \cdot mT_r}{c}\right) \\ &\quad \cdot \exp\left\{-j\pi\mu\left[nT_s - \frac{2(R_{k0} - v_k \cdot mT_r)}{c}\right]\right\} \\ &\quad (n = 0, 1, \ldots, N-1; \quad m = 0, 1, \ldots, M-1.) \end{aligned} \tag{7}$$

where N is the number of sampling points of each echo pulse, $T_s = 1/f_s$ the sampling period, and f_s the sampling frequency. After coherent integration to the M HRRPs in (7), the integration result is obtained:

$$\begin{aligned} z(n_k, d) = FFT\left[y(n_k, m), M\right] &= a_k \sqrt{\mu T_p^2} \cdot \frac{\sin\left[\pi M\left(T_r f_{dk} - d/M\right)\right]}{\sin\left[\pi\left(T_r f_{dk} - d/M\right)\right]} \\ &\quad \cdot \exp[j\pi(M-1)T_r f_{dk}] \cdot \exp\left[-j\pi \cdot \frac{M-1}{M} d\right] \cdot \exp\left[j2\pi\left(\varphi_k + \frac{1}{8}\right)\right] \\ &\quad (d = 0, 1, \ldots, M-1; k = 1, 2, \ldots, K.) \end{aligned} \tag{8}$$

where $n_k = \mathrm{Round}\left[2\left(R_{k0} - v_k \cdot mT_r\right)/\left(cT_s\right)\right]$ is the sampling number of the k-th scatterer, Round$[\cdot]$ represents round off. While if

$$f_{dk} = l \cdot f_r + \frac{d}{M} \cdot f_r, \quad l = 0, \pm 1, \pm 2, \ldots; \quad d = 0, 1, \ldots, M-1. \tag{9}$$

where $f_r = 1/T_r$ is the pulse repetition frequency, and $z(n_k, d)$ reaches the maximum. It can be seen that if the range velocities of the scatterers are different, the target echoes will spread in Doppler and the range-Doppler image of the target is coming out [14].

3. ECHO CHARACTERISTICS

3.1. Differences of the Echoes between the Vessel and the Chaff

3.1.1. Doppler Frequency Spectra

Coherent radar can obtain the Doppler frequency spectra of the target echoes, and then the motion information of the target is obtained.

After the chaff is blasted into the sky, the density of chaff cloud decreases gradually while the radar cross section (RCS) grows bigger and bigger. The Doppler frequency spectrum of the chaff cloud is up to the drift velocity of the chaff cloud and the motion of single chaff as well. The horizontal velocity of the chaff has a certain distribution. It has been verified that in a certain time after the chaff is dispersed, the diffusion process of the chaff cloud could be seen as a stationary process, and the horizontal velocity of chaff obeys Gaussian distribution [5]:

$$p(v_c) = \frac{1}{\sqrt{2\pi}\sigma_c} \exp\left[-\frac{(v_c - \varepsilon)^2}{2\sigma_c^2}\right] \tag{10}$$

where v_c denotes the instantaneous horizontal velocity of single chaff, σ_c the standard deviation of v_c, and ε the mean value of v_c. The center frequency of the Doppler frequency spectra depends on ε and the width of the Doppler frequency spectra depends on σ_c. Generally, the Doppler frequency spectra width of the chaff cloud is about hundreds of KHz. Compared with the chaff echo, the energy of the target ship echo focuses on several strong scatterers, and the differences of the relative velocities between the strong scatterers are minuscule in a CPI. Therefore the Doppler frequency spectra width of the vessel is small, in other words, the Doppler frequency spectra of the vessel is intensive.

3.1.2. Range-Doppler Image

In terms of the range-Doppler image of the wideband coherent radar, when the chaff cloud disperses thoroughly, the energy of the range-Doppler image spreads evenly. For the reason that the distribution of the chaff in space is uniform and the velocity of single chaff is stochastic. On the contrary, the energy of the vessel's range-Doppler image spreads intensively. For one thing that the energy of the vessel's HRRP focuses on several strong scatterers [15], and for another the Doppler of these scatterers are approximate. Figure 1 shows the measured range-Doppler images of the chaff and a vessel. It can be seen that the Doppler spectra width of the chaff is about 50 Doppler cells, and the Doppler spectra width of the vessel is only about 5 Doppler cells. The energy distribution of chaff echo is even as well, while the energy of the vessel focuses on several range-Doppler cells. It can also be seen that the range-Doppler image of the chaff occupies more range-Doppler cells than that of the vessel.

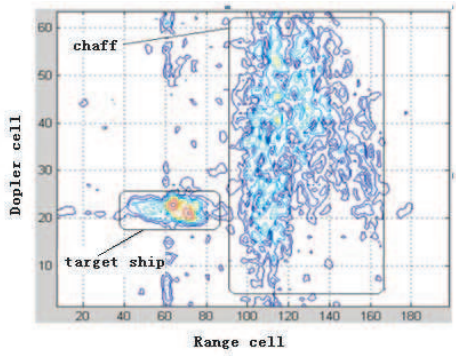

Figure 1. Range-Doppler images of the chaff and the vessel.

3.2. Features Extraction

After coherent integration and range-Doppler spread target detection [16], the range-Doppler image of the target can be obtained. (The range-Doppler spread target detection algorithm will be expounded in another paper.) By the measured data, Figure 2 shows the coherent integration result and the range-Doppler image of a vessel, and Figure 3 shows the coherent integration result and the range-Doppler image of the chaff.

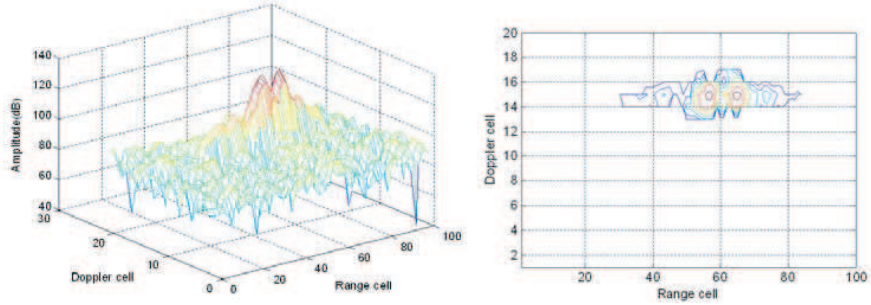

(a) (b)

Figure 2. Vessel echoes and the range-Doppler image. (a) Coherent integration result of the vessel echoes. (b) Range-Doppler image of the vessle.

3.2.1. Feature 1: Spread Factor of the Range-Doppler Image

Assume that the range-Doppler two-dimensional target detection window is W, with a length of L range cells and width of M Doppler

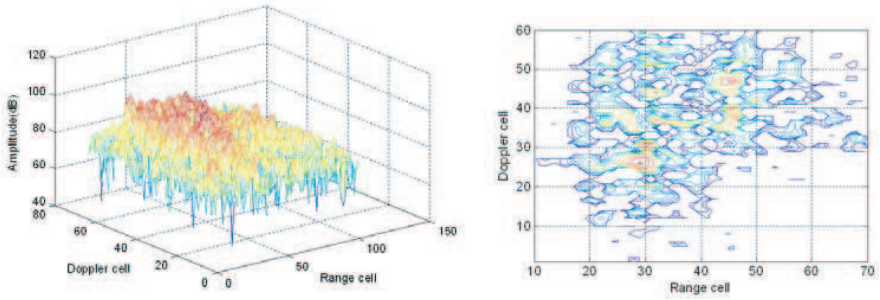

(a) (b)

Figure 3. Chaff echoes and the range-Doppler image. (a) Coherent integration result of the chaff echoes. (b) Range-Doppler image of the chaff.

cells. The range-Doppler image is represented as Θ, which is obtained by range-Doppler spread target detection. Setting that there are S range-Doppler cells contained in Θ, as a result, S can be seen as the area of the range-Doppler image Θ in the range-Doppler plane. As the analysis in Section 3.1, the Doppler frequency spectra width of the chaff is wider than that of the vessel, so the range-Doppler image of the chaff occupies more range-Doppler cells. While for the vessel, due to the echo characteristics, its range-Doppler image occupies less range-Doppler cells. The spread factor of the range-Doppler image is defined as:

$$\eta(\Theta)=\frac{\mathrm{S}}{\mathrm{L}\cdot\mathrm{M}} \tag{11}$$

The spread factor $\eta(\Theta)$ represents the relative area of the range-Doppler image occupying in the range-Doppler plane. From (11), it can be obtained:

$$0<\eta(\Theta)<1 \tag{12}$$

The smaller $\eta(\Theta)$ is, the more intensive the range-Doppler image will be. On the contrary, the greater $\eta(\Theta)$ is, the more disperse the range-Doppler image will be. Figure 4 shows the range-Doppler image spread factor of the vessel and the chaff with the measured data, where the horizontal axis is the trail number, and the ordinate axis is the spread factor, $L = 70$, and $M = 64$. It can be seen obviously that the spread factor of the chaff is greater than that of the vessel.

Table 1 shows some statistics of the range-Doppler image spread factors in Figure 4. As can be seen, the mean value of the spread factor of the chaff is much greater than that of the vessel. Yet the variation coefficient of the vessel is about 20%, and the variation coefficient of the chaff is 5.78%. The problem arises in part from that when the chaff

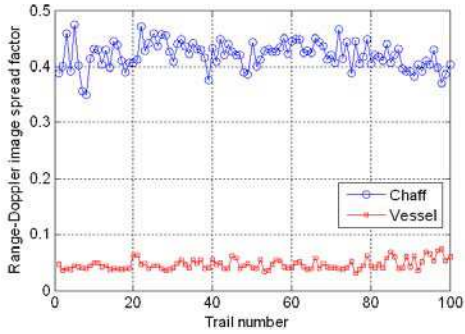

Figure 4. Range-Doppler image spread factors of the vessel and the chaff.

Table 1. Statistics of the spread factors in Figure 4.

Statistic	Mean value	Standard deviation	Variation coefficient
Chaff	0.4204	0.0243	5.78%
Vessel	0.0465	0.0093	20%

cloud disperses thoroughly, the echo of the chaff is relative steady, at the same time the echo of the vessel is violently varying between the CPI, especially when the observation angle of the radar changes.

3.2.2. Feature 2: Normalized Waveform Entropy of the Range-Doppler Image

The waveform entropy (WE) is usually adopted to measure the energy evenness of a signal [17, 18]. However, the number of range-Doppler cells occupied by the range-Doppler image is generally not a constant, so the WE defined in [17] and [18] does not work anymore. Consequently, a new normalized waveform entropy (NWE) is defined here to measure the energy evenness of the range-Doppler image. Setting

$$\begin{cases} p(i) = |\Theta(i)| / \|\Theta\| \\ \|\Theta\| = \sum_{i=1}^{S} |\Theta(n)| \end{cases}, \quad i = 1, 2, \ldots, S. \tag{13}$$

The NWE of the range-Doppler image is defined as:

$$E[\Theta] = -\frac{1}{\log_2 S} \sum_{i=1}^{S} p(i) \cdot \log_2 p(i) \tag{14}$$

According to the definition above, the NWE has the following properties:

(1) $E[\Theta] \geq 0$, and $E[\Theta] \to 0$, while $p(i) \to 0$;

(2) $E[\Theta] \leq 1$, and $E[\Theta] = 1$, while $p(i) = 1/S$, $\forall i = 1, 2, \ldots, S$.

For a vessel, the echo energy of the range-Doppler image focuses on several range-Doppler cells, which results in a small value of $E[\Theta]$. Compared with a vessel, however, the chaff echo is homogeneous in range and Doppler, the evenness of the chaff echo corresponds to a great value of $E[\Theta]$. Figure 5 shows the NWE of the range-Doppler image of the vessel and chaff with the measured data, where the horizontal axis is the trail number, and the ordinate axis is the NWE. It can be seen that the NWE of the chaff is greater than that of the vessel.

Table 2 shows some statistics of the NWEs in Figure 5. It can be seen that the mean value of the NWE of the chaff is 0.9343, and the variation coefficient is 0.57%, which means that the energy evenness of the range-Doppler image of the chaff and the stability are good. On the other hand, the NWE of the range-Doppler image of the vessel is 0.678, and the variation coefficient is 7.85%, which indicates that the energy distribution of range-Doppler image of the vessel is heterogeneous, and the stability is poor. The results in Table 2 correspond to the echo characters of the chaff and the vessel analyzed in the last section.

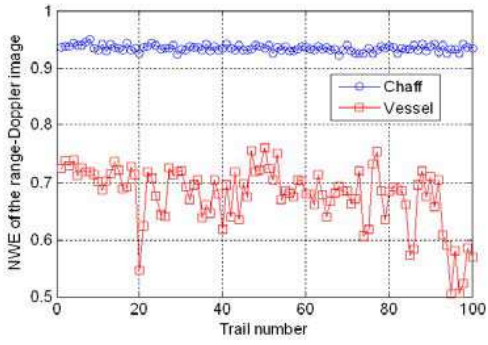

Figure 5. The NWEs of the range-Doppler image.

Table 2. Statistics of the NWEs in Figure 5.

Statistics	Mean value	Standard deviation	Variation coefficient
Chaff	0.9343	0.0053	0.57%
Vessel	0.6780	0.0532	7.85%

4. STATISTICAL ANALYSIS ON THE FEATURES

The two features extracted in Section 3.2 can be used to distinguish the vessel and chaff. The judgement thresholds of the features can be obtained by the experimental data and the required object identification performance of the radar system. Setting the judgement threshold of the spread factor and the NWE of the range-Doppler image are λ_1 and λ_2, respectively, which can be expressed as

$$\eta(\Theta) \underset{vessell}{\overset{chaff}{\gtrless}} \lambda_1 \tag{15}$$

$$and \qquad E(\Theta) \underset{vessel}{\overset{chaff}{\gtrless}} \lambda_2 \tag{16}$$

In order to analyze the probability distribution functions (PDF) of the two features, several classical PDFs are chosen to fit the real probability distribution by the measured data. We adopt the mean square error (MSE) to refine the approximation between the real distribution functions and the classical PDFs. Assuming that the real distribution function is p_0, the classical probability density function is p_1, and then the MSE between them can be expressed as:

$$c_{mse} = \|p_1 - p_0\|_2 \tag{17}$$

where $\|\cdot\|_2$ is the norm of ℓ_2.

Figure 6 shows the real data PDFs of the two features and the classical PDFs, which contain Gaussian, Rayleigh, Weibull and Logarithmic normal distribution [19]. Table 3 shows the MSE between the real distribution function and the classical PDFs. It can be seen that Lognormal distribution has the minimum MSE with the real distribution of the feature 1 of the vessel. As a result, we suppose that feature 1 of the vessel obeys Lognormal distribution. Similarly, feature 1 of the chaff, feature 2 of the vessel, and feature 2 of the chaff approximately obey Gaussian distribution, Weibull distribution, and Lognormal distribution, respectively.

False alarm probability is defined as the probability of the misjudgement considering the vessel as chaff jamming. Figure 7 shows the chaff identification performance of feature 1, where Figure 7(a) shows the relationship of the judgement threshold λ_1 and the false alarm probability p_{f1}, and Figure 7(b) shows the relationship of λ_1 and the chaff identification probability p_{d1}. Figure 8 shows the chaff identification performance of feature 2, where Figure 8(a)

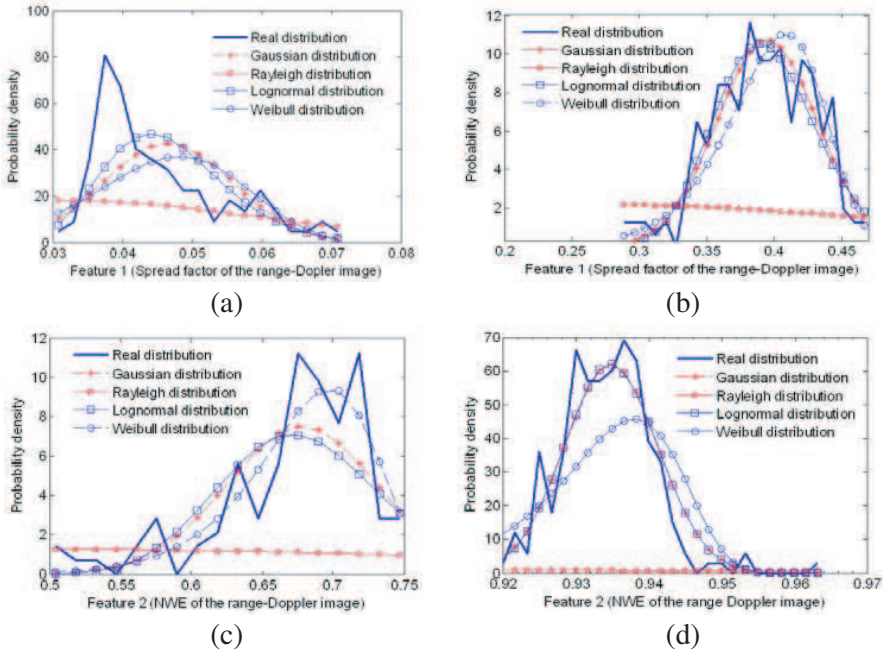

Figure 6. PDFs of the two features of the vessel and the chaff. (a) Feature 1 of the vessel. (b) Feature 1 of the chaff. (c) Feature 2 of the vessel. (d) Feature 2 of the chaff.

Table 3. The MSE between real distribution and the classical PDFs.

Features		Gaussian distribution	Rayleigh distribution	Lognormal distribution	Weibull distribution
Feature 1	Vessel	317.74	447.98	**245.60**	342.52
	Chaff	**2.22**	26.26	2.30	3.04
Feature 2	Vessel	4.74	21.30	5.69	**2.76**
	Chaff	55.99	1017.10	**55.52**	186.92

shows the relationship of the judgement threshold λ_2 and the false alarm probability p_{f2}, and Figure 8(b) shows the relationship of λ_2 and the chaff identification probability p_{d2}. Assuming that the required chaff identification probability is $1 - 10^{-5}$, namely $p_{d1} = p_{d2} = 1 - 10^{-5}$, the corresponding judgement thresholds can be obtained by straightforward computation: $\lambda_1 = 0.2366$, $\lambda_2 = 0.8969$. From Figure 7(a) and Figure 8(a), we can obtain $p_{fa1} < 10^{-14}$, and $p_{fa2} < 10^{-14}$, which indicates that proposed two features can be used

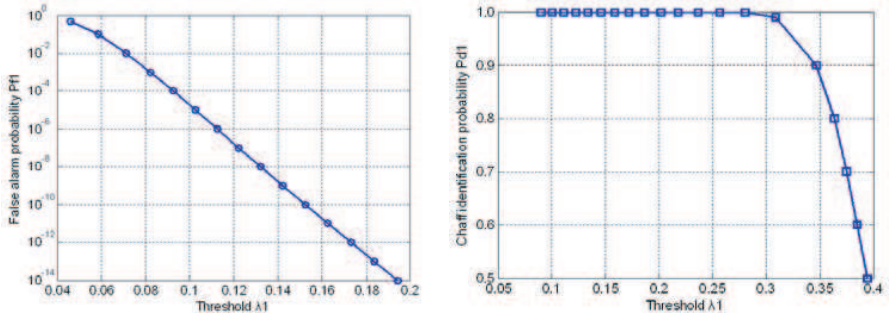

(a) (b)

Figure 7. Anti-chaff jamming performance of feature 1. (a) False alarm probability of λ_1. (b) Chaff identification probability of λ_1.

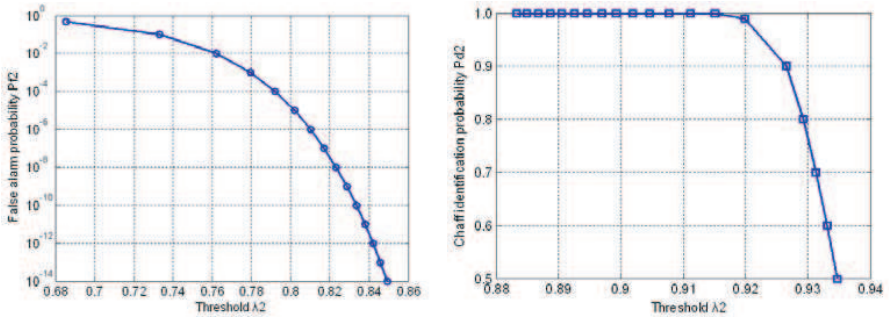

(a) (b)

Figure 8. Anti-chaff jamming performance of feature 2. (a) False alarm probability of λ_2. (b) Chaff identification probability of λ_2.

to distinguish the vessel and the chaff effectively, and may be adopted for chaff jamming identification for wideband coherent radars.

5. CONCLUSION

Chaff is still an effective defensive measure against anti-ship missiles and is widely adopted by Naval Force. Due to the working environment, the anti-chaff jamming technology of missile-borne terminal guidance radar is still imperfect. Wideband coherent LFM pulses radar has combination advantages of the wideband radar and the coherent radar, and has been widely used in terminal guidance. To study effective anti-chaff jamming method for wideband LFM coherent pulses radars, we investigate the echo characteristics of the vessel and

chaff in the distraction decoy and (or) the dump mode. Based on the measured data, the differences of the echoes between the vessel and the chaff are analyzed. In terms of the spread characteristic and energy evenness of the range-Doppler image, two features, namely, spread factor $\eta(\Theta)$ and normalized waveform entropy $E[\Theta]$ of the range-Doppler image, are proposed to distinguish the vessel and the chaff. Statistical distribution characteristics of the two features are investigated, and we find that the proposed features of the range-Doppler image can be used for chaff jamming identification for the wideband coherent radar. The robustness of the proposed method in variable signal to noise ratio (SNR) and the requirements on range and Doppler resolution will be analyzed in our future work.

ACKNOWLEDGMENT

The authors wish to thank the editors, reviewer 1 and reviewer 2, whose comments and suggestions helped to improve the contents of the paper.

REFERENCES

1. Macedo, A. D. F., "Analysis of chaff cloud RCS applying fuzzy calculus," *SBMO/IEEE MTT-S International Microwave and Optoelectronics Conference Proceedings*, Vol. 2, 724–728, 1997.
2. Fu, X., H. Yan, C. Jiang, and M. Gao, "Chaff jamming recognition for anti-vessel end-guidance radars," *Proceedings of the 2009 2nd International Congress on Image and Signal Processing, CISP'09*, Article No. 5304639, 2009.
3. Jia, X. and G. R. Guo, "Anti-chaff jamming method for anti-ship missile terminal guidance radar," *Shipboard Electronic Countermeasure*, Vol. 3, No. 3, 21–22, 1998.
4. Fu, H. W., S. W. Zhang, and X. M. Li, "A recognition method of chaff jamming based on gray principle," *Electronics Optics & Control*, Vol. 10, No. 3, 42–44, 2003.
5. Shang, W., B. X. Chen, and L. F. Jiang, "An anti-chaff jamming method based on the effect of spectral expansion," *Guidance & Fuze*, Vol. 27, No. 3, 5–10, 2006.
6. Shao, X. H., H. Du, and J. H. Xue, "A recognition method depended on enlarge the difference between target and chaff," *International Conference on Microwave and Millimeter Wave Technology, ICMMT'07*, Article No. 4266269, 2007.

7. Chua, M. Y. and V. C. Koo, "FPGA-based chirp generator for high resolution UAV SAR," *Progress In Electromagnetics Research*, Vol. 99, 71–88, 2009.
8. Chen, J., *Principles of Radar Passive Jamming*, 161–164, National Defense Industry Press, Beijing, 2009.
9. Wicks, M. C., E. L. Mokole, S. D. Blunt, R. S. Schneible, and V. J. Amuso, *Principles of Waveform. Diversity and Design*, Chap. 1, Scitech Publishing Inc., Mendham, New Jersey, 2010.
10. Farina, A. and F. A. Studer, "Detection with high resolution radar: Great promise, big challenge," *Journal of Systems Engineering and Electronics*, Vol. 3, No. 1, 21–34, 1992.
11. Wehner, D. R., *High-resolution Radar*, Chap. 4–Chap. 5, Artech House, Boston, 1995.
12. Tao, R., N. Zhang, and Y. Wang, "Analyzing and compensating the effects of range and Doppler frequency migrations in linear frequency modulation pulse compression radar," *IET Radar Sonar and Navigation*, Vol. 5, No. 1, 12–22, 2011.
13. Liu, B. and W. Chang, "Range alignment and motion compensation for missile-borne frequency stepped chirp radar," *Progress In Electromagnetics Research*, Vol. 136, 523–542, 2013.
14. Calvo-Gallego, J. and F. P**é**rez-Mart**í**nez, "Simple traffic surveillance system based on range-Doppler radar images," *Progress In Electromagnetics Research*, Vol. 125, 343–364, 2012.
15. Xia, G. F., H. C. Zhu, and H. Y. Su, "Research on the anti-chaff-interference for modulated stepped frequency terminal guided radar," *Radar Science and Technology*, Vol. 7, No. 1, 14–17, 2009.
16. Liu, B. and W. Chang, "A novel range-spread target detection approach for frequency stepped chirp radar," *Progress In Electromagnetics Research*, Vol. 131, 275–292, 2012.
17. Xi, L., "Auto focusing of ISAR images based on entropy minimization," *IEEE Trans. Aerospace Electron. Syst.*, Vol. 35, No. 4, 1240–1252, 1999.
18. Xu, S., P. Shui, and X. Yan, "CFAR detection of range-spread target in white Gaussian noise using waveform entropy," *Electronics Letters*, Vol. 46, No. 9, 647–649, 2010.
19. Chen, X. R. and Z. G. Zheng, *Modern Mathematics Handbook: Stochastic Mathematics,* 38–46, Huazhong University of Science and Technology Press, 1999.